Attitude Determination GPS/INS Integration System Design Using Triple Difference Technique

Sang Heon Oh*, Dong-Hwan Hwang[†], Chansik Park** and Sang Jeong Lee***

Abstract – GPS attitude outputs or carrier phase observables can be effectively utilized to compensate the attitude error of the strapdown inertial navigation system. However, when the integer ambiguity is not correctly resolved and/or a cycle slip occurs, an erroneous GPS output can be obtained. If the erroneous GPS output is applied to the attitude determination GPS/INS (ADGPS/INS) integrated navigation system, the performance of the system can be degraded. This paper proposes an ADGPS/INS integration system using the triple difference carrier phase observables. The proposed integration system contains a cycle slip detection algorithm, in which the inertial information is combined. Computer simulations and flight test were performed to verify effectiveness of the proposed navigation system. Results show that the proposed system gives an accurate and reliable navigation solution even when the integer ambiguity is not correctly resolved and the cycle slip occurs.

Keywords: Attitude determination, GPS, INS, Triple difference

1. Introduction

The attitude determination GPS (ADGPS) receiver can provide attitude output using carrier phase observables from multiple antennas [1, 2]. The GPS attitude output has bounded error characteristic as the position and velocity output from the GPS receiver [2]. In order to improve the performance of a navigation system, the GPS attitude output or carrier phase observable can be combined with the strapdown inertial navigation system (SDINS) outputs.

Several literatures can be found on the integration of the INS with the ADGPS receiver. Evans et al. [3] show a configuration of the integrated navigation system for an unmanned aerial vehicle (UAV) using an inertial measurement unit (IMU) and an ADGPS receiver as a subsystem of the autopilot system in the 'DragonFly' project. Wolf et al. [4] describe an integrated GPS/INS system that consists of a low cost IMU and an ADGPS receiver, 'TANS Vector' from Trimble Navigation Ltd. Gelderloos et al. [5] discussed a GPS attitude system integrated with inertial sensors for space applications. Gebre-Egziabher et al. [6] have introduced an inexpensive attitude heading reference system (AHRS), in which low cost automotive grade inertial sensors are integrated with an ADGPS receiver with ultra-short baseline antenna scheme.

In general, the carrier phase observable model is

composed of true range, integer ambiguity and error terms such as tropospheric delay, ionospheric delay, receiver clock error, multi-path error and receiver noise [7, 8]. The single difference between receivers or the double difference between receivers and satellites can eliminate some error terms in the carrier phase observable. However, the integer ambiguity cannot be removed by these methods and should be resolved before the integrated navigation system utilizes carrier phase observables [1, 9]. When the GPS attitude outputs and/or carrier phase observables contain incorrect integer ambiguity resolution and/or the cycle slip occurs, the ADGPS/INS integrated navigation system, may not give a desirable output. In order to guarantee a reliable and accurate navigation solution, a new integration algorithm is required to overcome the integer ambiguity error and the cycle slip.

The time differenced carrier phase measurements have been used for aiding in the GPS/INS integration system in order to avoid the hard ambiguity resolution problem. Wendel [10] and Soon [11] proposed a tightly coupled GPS/INS integration system with the time differenced carrier phase measurement in order to improve position accuracy. Grass and Lee [12] showed that high-accuracy differential positioning results can be obtained by using iterative double difference processing with triple difference method. Another application of carrier phase measurements is the GPS attitude determination. For the same reason as the GPS/INS integration, several papers have proposed the GPS attitude determination method using the time difference of the double differenced carrier phase measurements [13-16]. As is well-known, the triple difference can be subject to significant noise corruption. If there is a cycle slip in the GPS receiver due to low signal to noise ratio or loss of lock of the carrier tracking loop, the

---

† Corresponding Author: Department of Electronics Engineering, Chungnam National University, Korea (dhhwang@cnu.ac.kr)
* Hanyang Navicom Co., Ltd., Korea (laborosh@hanyangnav.co.kr)
** Department of Electronics Engineering, Chungbuk National University, Korea (chansp@chungbuk.ac.kr)
*** Department of Electronics Engineering, Chungnam National University, Korea (eesjl@cnu.ac.kr)

receiver does not give an accurate attitude output [17, 18]. Therefore, these weaknesses should be overcome in order to use the advantage on the integer ambiguity of the time difference of the double differenced carrier phase measurement.

This paper proposes an ADGPS/INS integration system using the triple difference technique. To eliminate the integer ambiguity in the GPS carrier phase measurement, the triple difference carrier phase observable is used and a new form of measurement equation is derived for the integration Kalman filter. For the cycle slip, an inertial-integrated detection algorithm is included in the proposed integration system. When a cycle slip is detected, the navigation system does not use the carrier phase observable in the Kalman filter.

2. Structure of the Proposed Navigation System

Fig. 1 illustrates overall structure of the proposed navigation system. The integration algorithm consists of SDINS part, triple difference carrier phase (TDCP) generation part, Kalman filtering part, and cycle slip detection part. The SDINS part computes position, velocity, and attitude from measured accelerations and angular rates of the IMU. The TDCP generation part calculates the TDCP observables from the carrier phase measurements. The Kalman filtering part estimates SDINS errors using the position output, velocity output, attitude output, and TDCP observables from SDINS and GPS receiver.

15 states error model is used for the Kalman filter; position error, velocity error, attitude error, gyroscope error, and accelerometer error. The gyroscope and accelerometer errors are modeled as random bias [19]. The cycle slip is detected by comparing the measured carrier phase observables with the estimated from the output of the SDINS [20]. When the cycle slip is detected, the Kalman filter does not use TDCP observables in order to eliminate influence of the cycle slip.
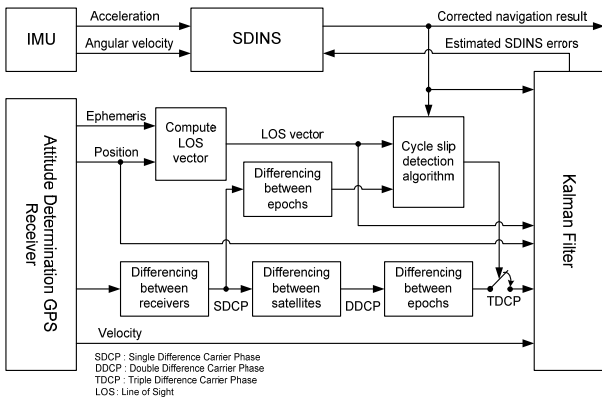

Fig. 1. Overall structure of the proposed integration system

3. Integration Algorithm

3.1 Carrier phase observable

Since the carrier phase observables have higher resolution and lower measurement noise than the code phase observables, they have been used for the high precision surveying and the attitude determination of vehicles with multiple GPS antennas. The relative positioning technique has been used for determination of vector between two receivers or antennas using the carrier phase observables. In this case, the difference technique is used for rejecting influence of the common errors contained in the undifferenced carrier phase observables [7, 8].

The undifferenced carrier phase observable can be modeled as

$$\lambda\Phi(k)^i_A = r^i_A(k) + \lambda N^i_A + cB^i_A + \delta^i_A + w^i_A(k) \tag{1}$$

where i and A denotes the satellite and GPS receiver (or antenna), respectively; λ represents wavelength of the L1 carrier and r^i_A is true range between the receiver (or antenna) A and the satellite i. N^i_A and cB^i_A denote integer ambiguity and receiver clock bias, respectively; δ^i_A is the carrier phase error that includes the ephemeris error, ionospheric advance and tropospheric delay and w^i_A is the measurement noise that includes the multipath error and receiver noise.

The double difference technique has been used for attitude determination because it can remove receiver clock bias and other common errors except for the integer ambiguity and measurement noise [2]. The double difference carrier phase (DDCP) observable between two antennas is given by

$$\lambda\Phi^{ij}_{MS} \equiv \lambda\left\{\left[\Phi^j_S(k) - \Phi^j_M(k)\right] - \left[\Phi^i_S(k) - \Phi^i_M(k)\right]\right\}$$
$$= r^{ij}_{MS}(k) + \lambda N^{ij}_{MS} + w^{ij}_{MS}(k) \tag{2}$$

where i and j denote satellites; M denotes the master antenna and S the slave antenna. r^{ij}_{MS} is double differenced true range; N^{ij}_{MS} and w^{ij}_{MS} are the double differenced integer ambiguity and measurement noise, respectively. Linearizing (2) at the master antenna position gives

$$l^{ij}_{MS}(k) = h^{ij}_M(k)r^e(k) + \lambda N^{ij}_{MS} + w^{ij}_{MS}(k) \tag{3}$$

where l^{ij}_{MS} denotes linearized DDCP observable; h^{ij}_M is difference between the line-of-sight (LOS) vectors from the master antenna to satellite i and satellite j; r^e is the baseline vector from the master antenna to the slave

antenna in the earth centered earth fixed (ECEF) frame.

Let us define $\Delta x(k) \equiv x(k) - x(k-1)$ for a variable x. The linearized TDCP observable (4) can be obtained by differencing (3) between the k th epoch and the $(k-1)$ th epoch.

$$
\begin{aligned}
\Delta l_{MS}^{ij}(k) &\equiv l_{MS}^{ij}(k) - l_{MS}^{ij}(k-1) \\
&= h_M^{ij}(k)r^e(k) - h_M^{ij}(k-1)r^e(k-1) \\
&\quad + w_{MS}^{ij}(k) - w_{MS}^{ij}(k-1) \\
&= h_M^{ij}(k)r^e(k) - h_M^{ij}(k-1)r^e(k-1) + \Delta w_{MS}^{ij}(k)
\end{aligned}
\tag{4}
$$

If no cycle slips have occurred in the carrier phase observables, the integer ambiguity is removed from the DDCP observables in (3). In the proposed integration scheme, the TDCP observables are used for measurements of the Kalman filter. The measurement equation for the Kalman filter is derived in the following subsection.

3.2 Kalman filter for integration

The error model for the Kalman filter [19, 21] is described by

$$
\dot{\mathbf{x}}(t) = \mathbf{F}(t)\mathbf{x}(t) + \mathbf{w}(t), \ \mathbf{w}(t) \sim N(0, \ \mathbf{Q}(t))
$$
$$
\begin{bmatrix} \dot{\mathbf{x}}_{nav} \\ \dot{\mathbf{x}}_{sensor} \end{bmatrix} = \begin{bmatrix} \mathbf{F}_{11} & \mathbf{F}_{12} \\ \mathbf{0}_{6\times 9} & \mathbf{0}_{6\times 6} \end{bmatrix} \begin{bmatrix} \mathbf{x}_{nav} \\ \mathbf{x}_{sensor} \end{bmatrix} + \begin{bmatrix} \mathbf{w}_{nav} \\ \mathbf{w}_{sensor} \end{bmatrix}
\tag{5}
$$

where $\mathbf{x}_{nav}$ and $\mathbf{x}_{sensor}$ are the navigation and sensor error state vector, respectively. The navigation error state vector consists of position, velocity, and attitude error which is derived in the psi angle error model. The sensor error state vector consists of accelerometer and gyro error which are modeled as random biases.

The measurement equation is described by

$$
\mathbf{z}(t) = \mathbf{H}(t)\mathbf{x}(t) + \mathbf{v}(t), \ \mathbf{v}(t) \sim N(0, \ \mathbf{R}(t))
$$
$$
\mathbf{z} = \begin{bmatrix} \mathbf{z}_1 \\ \mathbf{z}_2 \end{bmatrix} = \begin{bmatrix} \mathbf{H}_1 \\ \mathbf{H}_2 \end{bmatrix} \mathbf{x} + \begin{bmatrix} \mathbf{v}_1 \\ \mathbf{v}_2 \end{bmatrix}
\tag{6}
$$

where $\mathbf{H}_1$ is the measurement sub matrix related to the position and velocity error and $\mathbf{H}_2$ the TDCP observables.

In order to derive the measurement equation for the integration Kalman filter, the followings are assumed.

Assumption 1. There is no variation in the LOS vector between two consecutive epochs.

$$
h_M^{ij}(k) \cong h_M^{ij}(k-1)
\tag{7}
$$

Remark 1
Difference of the LOS vector between two consecutive

epochs is

$$
\Delta h_M^{ij}(k) = h_M^{ij}(k) - h_M^{ij}(k-1)
\tag{8}
$$

Substituting (8) into (4), the linearized TDCP observable model can be rewritten as follows

$$
\begin{aligned}
\Delta l_{MS}^{ij}(k) &= h_M^{ij}(k)r^e(k) - h_M^{ij}(k-1)r^e(k-1) + \Delta w_{MS}^{ij}(k) \\
&= h_M^{ij}(k)r^e(k) \\
&\quad - \left[h_M^{ij}(k) - \Delta h_M^{ij}(k) \right] r^e(k-1) + \Delta w_{MS}^{ij}(k) \\
&= h_M^{ij}(k)\left[r^e(k) - r^e(k-1) \right] \\
&\quad + \Delta h_M^{ij}(k)r^e(k-1) + \Delta w_{MS}^{ij}(k)
\end{aligned}
\tag{9}
$$

In order to investigate influence of the second term $\Delta h_M^{ij}(k)r^e(k-1)$, in the linearized triple difference model in (9), a simulation was performed. In the simulation, the Matlab® and Satellite Navigation Toolbox from GPSoft were used to generate motion of the GPS satellites [22]. Fig. 2 illustrates arrangement of antennas for the ADGPS receiver. Motion of the GPS satellites was simulated from 1,000 to 3,000 second of GPS time when the ADGPS receiver stays at 45° north latitude, 45° east longitude, and 0 m altitude. In this case, all antennas can observe at least 6 satellites when the mask angle is set to be 15°.

Using the Cauchy-Schwarz inequality [23], the inner product of $\Delta h_M^{ij}(k)$ and $r^e(k-1)$ can be written as (10).

$$
\left| \Delta h_M^{ij}(k)r^e(k-1) \right| \leq \left\| \Delta h_M^{ij}(k) \right\| \left\| r^e(k-1) \right\|
\tag{10}
$$

Note that the norm (length) of the baseline vector $r^e(k-1)$ does not change and is 1 m in Fig. 2.
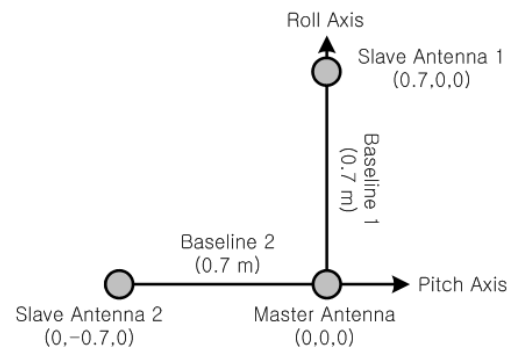

Fig. 2. Arrangement of GPS antennas

Fig. 3 shows variation of the norm of $\Delta h_M^{ij}(k)$ during the simulation interval. The legend (i, j) denotes PRN number of the satellite.

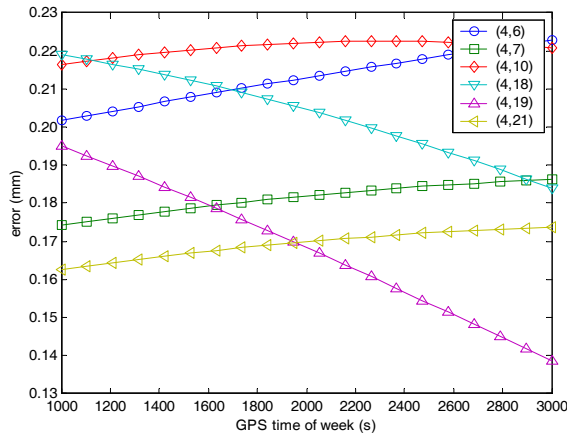In Fig. 3, it can be observed that all the norms of

Fig. 3. Variation of norm of the LOS vector

$\Delta h_M^{ij}(k)$ for satellites are less than 3.0×10^{-4}. From the inequality (10) and the simulation result, maximum variation of the TDCP observable caused by the $\Delta h_M^{ij}(k)$ is less than 3.0×10^{-4} m. Magnitude of the GPS carrier phase measurement noise is known to be approximately 1.9×10^{-3} m at the L1 frequency [24]. Magnitude of the TDCP observable measurement noise is approximately 5.4×10^{-3} m since magnitude of the TDCP observable measurement noise is $2\sqrt{2}$ times that of the undifferenced. As a result of this, influence of the second term $\Delta h_M^{ij}(k)r^e(k-1)$ can be neglected in the linearized triple difference model in (9) since it is sufficiently small value compared with the measurement noise of the TDCP observable. From the above observation, the assumption 1 can be acceptable in real applications.

Assumption 2. *There is no variation in the C_n^e matrix between two consecutive epochs.*

$$C_n^e(k) \cong C_n^e(k-1) \tag{11}$$

where C_n^e is the coordinate transformation matrix from the navigation frame to the ECEF frame (*e* frame).

Remark 2
If a vehicle moves in a very high speed, for example, 1,000 km/h (=277.8 m/s), change of the latitude or longitude is less than 10^{-4} rad in 1 s. Entries of the coordinate transformation matrix C_n^e are expressed in sums and multiplications of the trigonometric functions, in which independent variables are latitude and longitude of the vehicle. Variation of each entry value is small enough to ignore. From this observation, the assumption 2 can be acceptable in real situation.

Assumption 3. *There is no variation in the SDINS attitude error between two consecutive epochs.*

$$\delta\psi(k) \cong \delta\psi(k-1) \tag{12}$$

where $\delta\psi$ is the SDINS attitude error vector defined by the psi angle error model [24].

Remark 3
It is well known that the SDINS attitude error oscillates in Schuler frequency with 84 minutes period [25]. It can be assumed that the SDINS attitude error does not change between two consecutive epochs as in the assumption 3.

The TDCP observable can be rewritten from (4) using the assumption 1 as follows

$$\begin{aligned}
\Delta l_{MS}^{ij}(k) &= h_M^{ij}(k)r^e(k) - h_M^{ij}(k-1)r^e(k-1) + \Delta w_{MS}^{ij}(k) \\
&\cong h_M^{ij}(k)\left[r^e(k) - r^e(k-1)\right] + \Delta w_{MS}^{ij}(k) \\
&= h_M^{ij}(k)\Delta r^e(k) + \Delta w_{MS}^{ij}(k)
\end{aligned} \tag{13}$$

The measurement equation can be derived from the estimate expression of the TDCP observable from the output of the SDINS. The baseline vector can be expressed as (14) in terms of the attitude error of the SDINS introduced in (5).

$$\begin{aligned}
r^e &= C_n^e r^n = C_n^e C_b^n r^b = C_n^e\left[I + \delta\psi^\times\right]\bar{C}_b^n r^b \\
&= C_n^e \bar{C}_b^n r^b + C_n^e \delta\psi^\times \bar{C}_b^n r^b \\
&= C_n^e \bar{C}_b^n r^b - C_n^e\left(\bar{r}^n\right)^\times \delta\psi
\end{aligned} \tag{14}$$

where $\bar{C}_b^n$ is the estimated coordinate transformation matrix from the body frame to the navigation frame; r^b and $\bar{r}^n$ are the baseline vector in the body frame and estimated baseline vector in the navigation frame, respectively. The over bar represents an estimated value from the SDINS output. The notation $(a)^\times$ means the skew-symmetric matrix of the a vector as (15).

$$(a)^\times = \left(\begin{bmatrix} \alpha \\ \beta \\ \gamma \end{bmatrix}\right)^\times = \begin{bmatrix} 0 & -\gamma & \beta \\ \gamma & 0 & -\alpha \\ -\beta & \alpha & 0 \end{bmatrix} \tag{15}$$

Difference of the baseline vector $\Delta r^e(k)$ can be expressed as (16) from (14) using the assumption 2 and 3

$$\begin{aligned}
\Delta r^e(k) &= r^e(k) - r^e(k-1) \\
&= C_n^e(k)\bar{C}_b^n(k)r^b - C_n^e(k-1)\bar{C}_b^n(k-1)r^b \\
&\quad - C_n^e(k)\left(\bar{r}^n(k)\right)^\times \delta\psi(k) \\
&\quad + C_n^e(k-1)\left(\bar{r}^n(k-1)\right)^\times \delta\psi(k-1) \\
&\cong C_n^e(k)\left[\bar{C}_b^n(k) - \bar{C}_b^n(k-1)\right]r^b \\
&\quad - C_n^e(k)\left[\left(\bar{r}^n(k)\right)^\times - \left(\bar{r}^n(k-1)\right)^\times\right]\delta\psi(k) \\
&= C_n^e(k)\Delta\bar{C}_b^n(k)r^b - C_n^e(k)\left(\Delta\bar{r}^n(k)\right)^\times \delta\psi(k)
\end{aligned} \tag{16}$$

From (13) and (16), the estimated TDCP observable can be expressed as

$$\overline{\Delta l_{MS}^{ij}}(k) = h_M^{ij}(k)\Delta r^e(k)$$
$$= h_M^{ij}(k)C_n^e(k)\Delta\overline{C}_b^n(k)r^b \qquad (17)$$
$$- h_M^{ij}(k)C_n^e(k)\left(\Delta\overline{r}^n(k)\right)^\times \delta\psi(k)$$

where the $\overline{\Delta l_{MS}^{ij}}$ denotes the estimated value of Δl_{MS}^{ij}.

In the indirect Kalman filter, state variables and measurement equation are expressed in terms of SDINS errors [18]. The TDCP measurement should be expressed in the SDINS attitude error. From (16) and (17), the measurement equation can be obtained as (18)

$$z^{ij} = \Delta l_{MS}^{ij} - \overline{\Delta l_{MS}^{ij}} = h_M^{ij}C_n^e\left(\Delta\overline{r}^n\right)^\times \delta\psi + v \qquad (18)$$

Hence, the part of the measurement equation related to the TDCP is given by

$$\mathbf{z}_2 = \mathbf{H}_2\mathbf{x} + \mathbf{v}_2$$
$$= \begin{bmatrix} 0_{(k-1)\times 6} & H_M C_n^e\left(\Delta\overline{r}^n\right)_1^\times & 0_{(k-1)\times 3} & 0_{(k-1)\times 3} \\ 0_{(k-1)\times 6} & H_M C_n^e\left(\Delta\overline{r}^n\right)_2^\times & 0_{(k-1)\times 3} & 0_{(k-1)\times 3} \\ \vdots & \vdots & \vdots & \vdots \\ 0_{(k-1)\times 6} & H_M C_n^e\left(\Delta\overline{r}^n\right)_l^\times & 0_{(k-1)\times 3} & 0_{(k-1)\times 3} \end{bmatrix}\mathbf{x} + \mathbf{v}_2 \qquad (19)$$
$$H_{M_{(k-1)\times 3}} = \left[\left(h_M^{12}\right)^T \quad \left(h_M^{13}\right)^T \quad \cdots \quad \left(h_M^{1k}\right)^T\right]^T \qquad (20)$$

where k and l denotes number of satellites in view to a baseline and number of baseline vectors, respectively.

In spite that the measurements noises are crossly correlated when the carrier phase observables are processed by triple difference technique [8], it is assumed that the measurement noises are white Gaussian random variables. Therefore, it is expected that performance of the integration Kalman filter be degraded. In order to take into consideration of this problem, value of the measurement noise covariance matrix $\mathbf{R}$ should be carefully tuned through simulations and post-mission data processing.

3.3 Cycle slip detection

Even though the integration system utilizes the TDCP observables, the cycle slip cannot be avoided. The cycle slip may give rise to performance degradation in integrated navigation systems. In order to cope with this problem, a cycle slip detection algorithm using inertial information [26] is included in the proposed integration algorithm. When a cycle slip is detected, the integration Kalman filter does not use the TDCP observables.

If the attitude determination GPS receiver uses one common clock, the single difference carrier phase observables between receivers is given by

$$l_{MS}^i(k) = h_M^i(k)r^e(k) + \lambda N_{MS}^i + w_{MS}^i(k) \qquad (21)$$

where h_M^i is the LOS vector from the master antenna M to the satellite i. Taking difference between two consecutive epochs in (21) and using the assumption 1 in the previous section gives (22).

$$\Delta l_{MS}^i(k) \cong h_M^i(k)\Delta r^e(k) + \Delta w_{MS}^j(k) \qquad (22)$$

The Δl_{MS}^i can be estimated from the estimated baseline vector $\Delta\overline{r}^e$.

$$\overline{\Delta l_{MS}^i}(k) \cong h_M^i(k)\Delta\overline{r}^e(k) \qquad (23)$$

The measurement of the integration Kalman filter is given by

$$\Delta l_{MS}^i(k) - \overline{\Delta l_{MS}^i}(k) \cong h_M^i(k)\left[\Delta r^e(k) - \Delta\overline{r}^e(k)\right]$$
$$+ \Delta w_{MS}^j(k) \qquad (24)$$
$$= h_M^i(k)\delta\Delta r^e(k) + \Delta w_{MS}^j(k)$$

where $\delta\Delta r^e$ is error of the estimated baseline vector.

The cycle slip is detected by using the following inequality (25).

$$\left|\Delta l_{MS}^i(k) - \overline{\Delta l_{MS}^i}(k)\right| > \varepsilon \qquad (25)$$

In the inequality (25), a threshold ε is selected from the baseline vector error and measurement noise in the carrier phase observables. Since measurement noise is generally less than 10 mm and the SDINS provides a very accurate navigation solution between two consecutive epochs, it can be expected that the cycle slip can be effectively detected using (25).

4. Computer Simulation

In order to investigate effectiveness of the proposed algorithm, computer simulations were performed. Error characteristics of an automotive grade IMU and L1 C/A code GPS which was given in Table 1 was used for the simulation. The Satellite Navigation Toolbox was used to simulate motion of the GPS satellites and generate the raw measurements and errors. The arrangement of the GPS antennas is illustrated in Fig. 2.

A flight path for the simulation is shown in Fig. 4 and 5. The vehicle is stationary for 30 seconds and accelerated

toward the north for 10 seconds. After that, it climbs for 15 seconds up toward 2.27 km altitude and performs two circular flights with 10 ° bank angle.

Table 1. Error Characteristics of IMU and GPS

		Error Source	1σ
IMU	Gyro	Bias (°/h)	3600.0
		Random Walk (°/√h)	2.25
	Accel	Bias (mg)	10.0
		Random Walk (m/s/√h)	0.15
GPS	Ionospheric Advance (m)		5.0
	Tropospheric Delay (m)		1.5
	Multipath (Pseudorange) (m)		1.5
	Multipath (Carrier Phase) (m)		1.5×10^{-2}
	Receiver noise (Pseudorange) (m)		1.5
	Receiver noise (Carrier Phase) (m)		1.9×10^{-3}
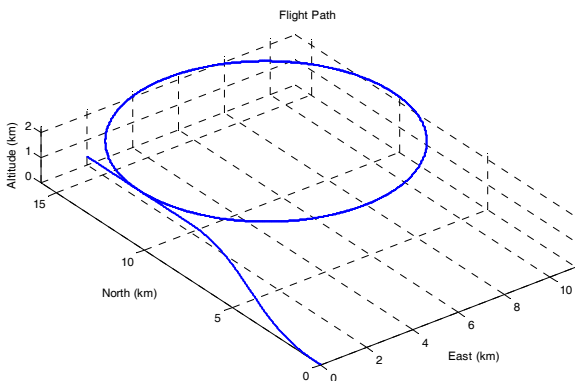
Fig. 4. Flight path for simulation
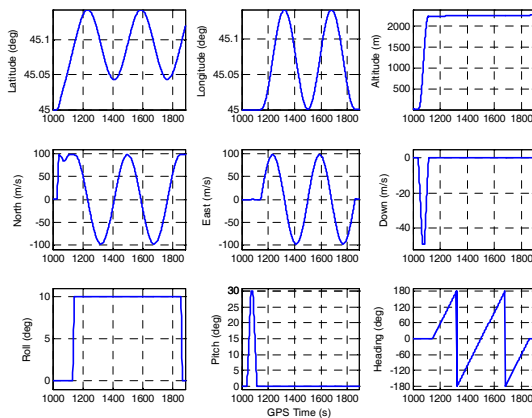
Fig. 5. Fight path

50 times Monte-Carlo simulations were carried out and incorrect integer ambiguity resolution was intentionally included to access performance of the proposed algorithm. At 1500 second (GPS time), the integer ambiguity of the DDCP observables of baseline 1 is incorrectly resolved from -60 to -59 due to the cycle slip. At this time, the incorrectly resolved integer ambiguity causes attitude error in the ADGPS receiver as shown in Fig. 6.
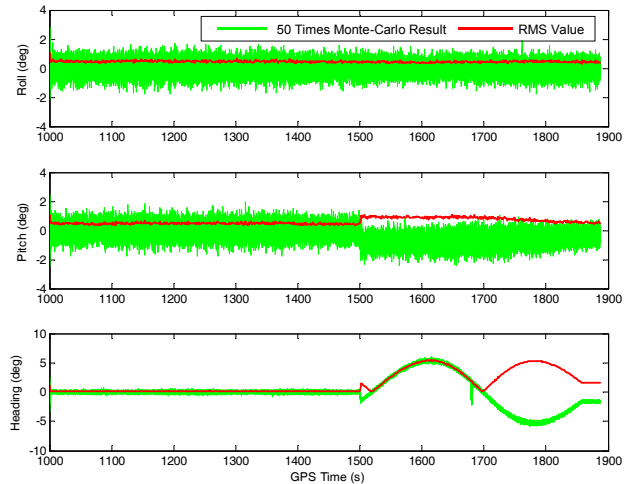

Fig. 6. Attitude error of ADGPS receiver during simulation

Maximum roll, pitch, and heading errors are 1.05°, 1.06°, and 5.41° root-mean-square (RMS), respectively. In general, attitude determination real-time software of an ADGPS receiver includes a cycle slip detection algorithm and a validation routine for resolved integer ambiguity. It takes from few seconds to several minutes to detect and correct the error of the integer ambiguity resolution. In this simulation, it is assumed that the ADGPS receiver cannot correct the integer ambiguity error for several minutes to evaluate performance of the proposed algorithm.

Simulation results are shown in Fig. 7 and 8. Figures show results of the conventional tightly coupled GPS/INS integration, the ADGPS/INS integration with DDCP observables, and the ADGPS/INS integration with TDCP observables proposed in this paper. In Fig. 7, the navigation error is the root-sum-square (RSS) value calculated from the RMS error of each axis of the navigation frame. In Fig. 8, the IMU bias estimation error is mean value of the RMS error of each axis of the body frame.

Each integration algorithm gives similar position and velocity accuracy as in Fig. 7. The tightly-coupled GPS/INS integration gives large attitude error in stationary state since the heading error greatly increases due to lack of observability. On the other hand, the ADGPS/INS integrations provide more accurate attitude result than tightly-coupled GPS/INS integration. After cycle slip, the incorrectly resolved integer ambiguity gives rise to large attitude error in the ADGPS/INS integration with DDCP. The proposed ADGPS/INS integration algorithm provides the most accurate attitude result since it is not affected by the integer ambiguity resolution.

In Fig. 8, it can be observed that the ADGPS/INS integration with DDCP provides the best bias estimation performance before cycle slip and the bias estimation error increases with time after cycle slip. The proposed integration algorithm gives approximately two times better bias estimation performance than the tightly-coupled
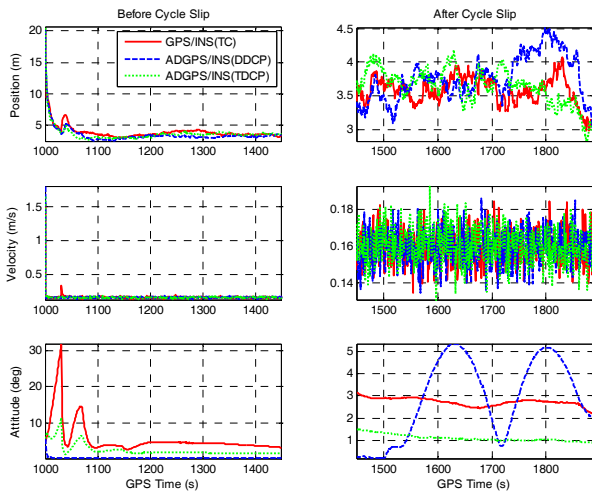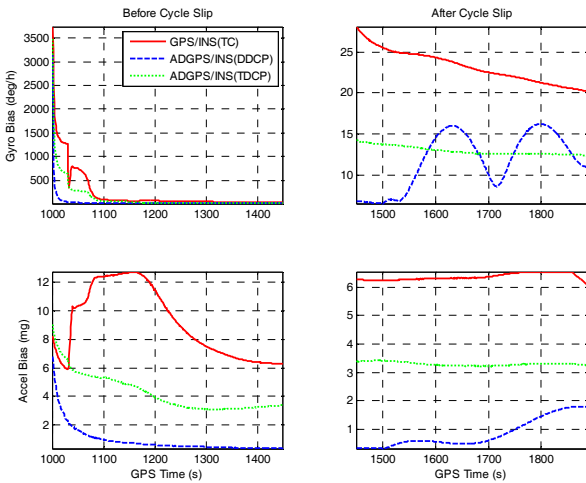
Fig. 7. Navigation error

Fig. 8. Bias estimation error

GPS/INS integration in spite of cycle slip occurrence.

3. Flight Test

To evaluate performance of the proposed algorithm, a flight test was performed. An experimental setup was installed in a four-seated small aircraft. For attitude determination, three aviation GPS antennas (manufactured by Sensor Systems Inc., S67-1575-490) are setup, with 0.7m length of baseline vector as shown in Fig. 9.

Fig. 10 shows installation of A commercial automotive grade IMU which was mounted on the longitudinal axis of the fuselage. The specification of the IMU is given in Table 2. A commercial data acquisition system was used to record raw data of sensors (GPS, IMU) in the test aircraft for post-mission data processing and performance analysis of the proposed algorithm.

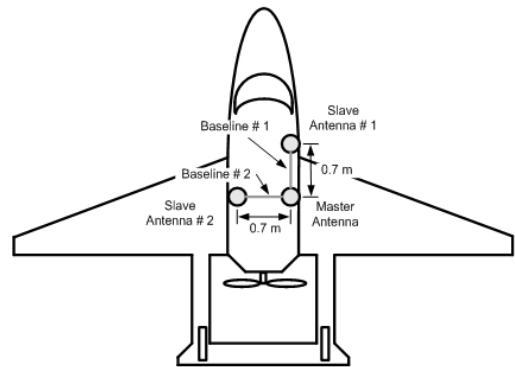The test aircraft conducted several types of maneuvering as shown in Fig. 11. Total flight distance was 55.5 km and
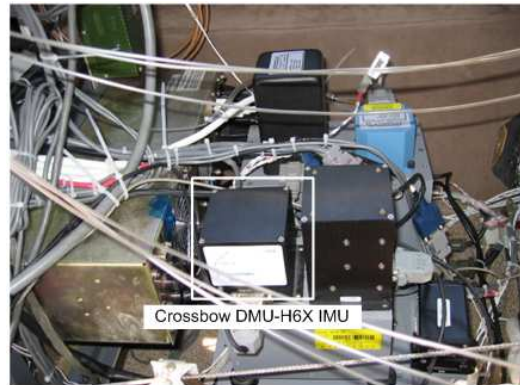

Fig. 9. Arrangement GPS antennas for flight test

Fig. 10. Installation of IMU

Table 2. Specification of IMU

	Item	Description
	Manufacturer	Crossbow, USA
	Model	DMU-H6X
	Grade	Automotive
	Gyro Type	MEMS
Gyro	Bias (°/h)	3600.0
	Random Walk (°/√h)	2.25
Accel	Bias (mg)	10.0
	Random Walk (m/s/√h)	0.15
	Interface	UART (RS-232)
	Output Rate (Hz)	200
	Size (mm)	76.2 × 95.3 × 81.3
	Power Consumption (W)	< 3

flight time 23 minutes. During the test, maximum ground speed and acceleration reached 252 km/h and 2 G, respectively.

After takeoff, the test aircraft went up to 620 m altitude for 100 seconds with 10° climb angle to enter the maneuvering region. In the maneuvering region, the test flight performed 2 sets of motion, banking and phugoid. During the phugoid motion, total altitude change was approximately 150 m. Subsequently, the test aircraft descended to 300 m altitude and conducted a straight and level flight with average 217 km/h ground speed for 240 seconds toward the vicinity of airfield. Finally, it performed 180° turning to approach the runway and landed

from the opposite direction of takeoff. The test flight profile is summarized in Table 3.
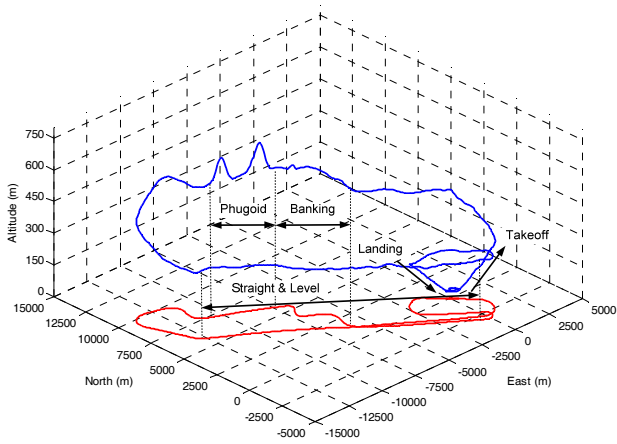

Fig. 11. Test flight path

Table 3. Type of maneuvering during flight test

Profile	Type of Maneuver	GPS Time (Duration)
1	±20° and ±50° Banking	111,329 ~ 111,423 s (94 s)
2	+20/-10° and +15/-10 ° Phugoid	111,424 ~ 111,499 s (75 s)
3	Straight and Level Flight	111,662 ~ 111,899 s (237 s)

Fig. 12 shows number of satellites in view at the master antenna and baselines. It can be seen that satellite visibility was good; maximum number of satellites in view was 8. On the runway, number of satellites in view was changed frequently due to signal blockage by the hangar. After takeoff, the number of satellite in view was 8. During the profile 1, number of common satellites in view of baselines dropped to 4 and changed into 7 during the profile 3. Number of common satellites in view of baselines decreased temporarily to 5 when the test aircraft conducted a banked turn to approach the runway. Number of common satellites in view of baselines recovered rapidly to 8 during landing.

Since a highly accurate navigation system, which can be regarded as a reference navigation system for performance evaluation, could not be installed in the test aircraft, the proposed integrated navigation system was evaluated by observing navigation output differences between the ADGPS receiver and each integration algorithm. The
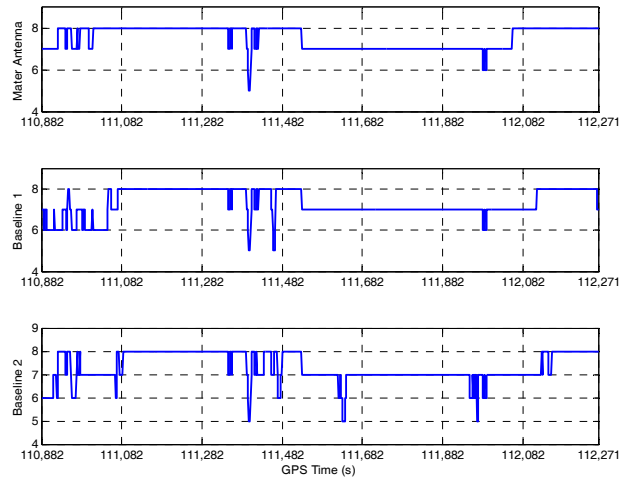

Fig. 12. Number of satellites in view during flight test

navigation output differences between the ADGPS receiver and integration algorithms are given in Table 4. It can be observed that there were no significant differences in navigation performance.

Roll and pitch outputs were compared with those of a vertical gyroscope. The vertical gyroscope used in the evaluation was the Aeronetic RVG-801E vertical gyroscope which provides roll and pitch angle at 50 Hz with ±0.5° RMS error.

Fig. 13 shows outputs of the navigation systems for ±20° and ±50° roll motion. The ADGPS receiver doses not provide accurate roll output due to incorrectly resolved integer ambiguity during -50° roll motion. In this case, the ADGPS/INS integration with DDCP gives maximum 20.5° roll error with respect to the output of the vertical gyroscope. On the other hand, the output of the proposed algorithm is not affected by integer ambiguity resolution error.

Outputs of the navigation systems for +20/-10° and +15/-10° pitch motion are shown in Fig. 14. The ADGPS/INS integration with DDCP gives maximum 13.4° pitch error when the ADGPS receiver provides incorrect attitude. It can be seen that pitch error of the proposed algorithm doses not exceed 2.3°.

Fig. 15 shows the heading output in early stage of the flight test. It can be observed that the heading error of tightly-coupled GPS/INS integration increases rapidly in the stationary state. The rate of the heading error of the

Table 4. Navigation output results

		GPS/INS (TC)		ADGPS/INS (DDCP)		ADGPS/INS (TDCP)	
		Mean	STD	Mean	STD	Mean	STD
Position (m)	North	0.204	2.868	0.205	2.864	0.419	2.915
	East	-0.330	2.346	-0.328	2.345	-0.256	2.423
	Down	-0.054	5.170	-0.053	5.173	-0.053	5.177
Velocity (m/s)	North	0.025	0.365	0.027	0.370	0.030	0.379
	East	-0.001	0.414	-0.001	0.420	0.001	0.389
	Down	0.045	0.942	0.043	0.941	0.044	0.944
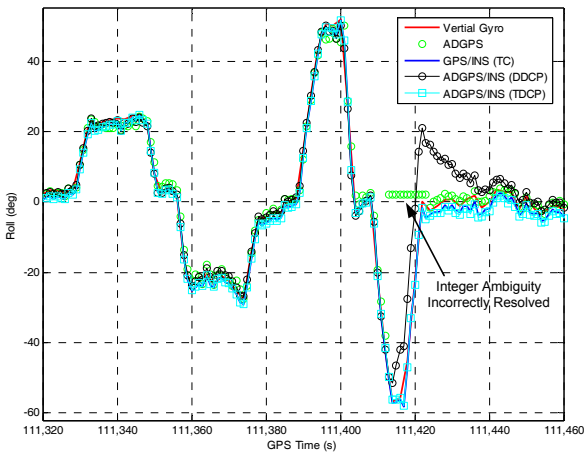
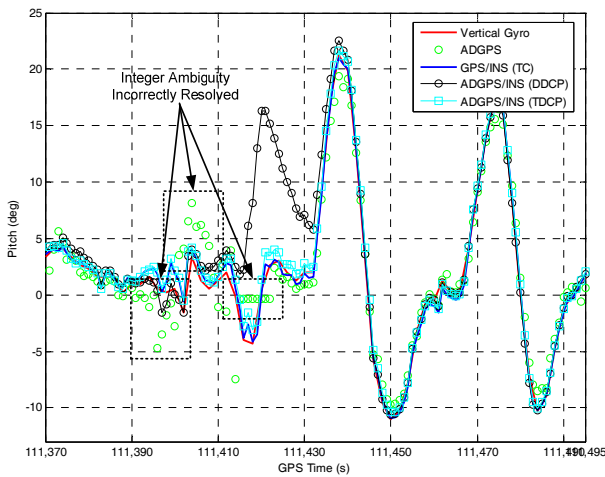**Fig. 13.** Outputs for ±20° and ±50° roll motion

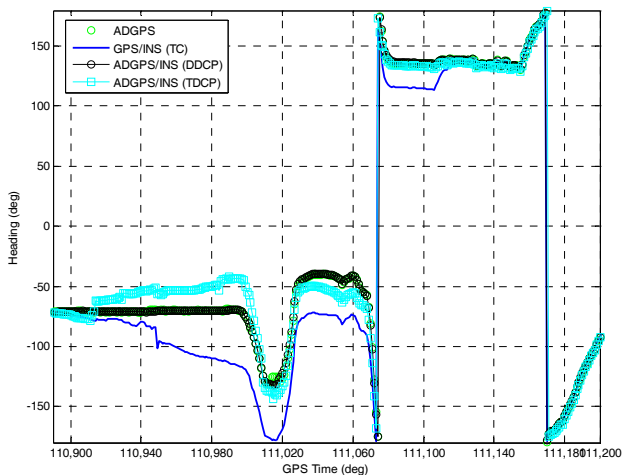**Fig. 14.** Output for +20/-10 ° and +15/-10 ° pitch motion (phugoid)

Fig. 15. Heading output in early stage of the flight test

proposed algorithm is relatively lower than that of the tightly coupled GPS/INS integration even in stationary state. After initial heading motion, the heading result of the

proposed algorithm follows that of the ADGPS receiver as same case as the ADGPS/INS integration with DDCP.

The heading outputs during roll motion are shown in Fig. 16. Difference of heading output between the tightly-coupled GPS/INS integration and the ADGPS receiver increases gradually when the test aircraft performs straight and level flight from 111,240 to 111,320 second (GPS time). The large heading error can be observed in the ADGPS/INS integration with DDCP when the ADGPS receiver gives incorrect attitude output. It can also be observed that the proposed integration algorithm provides an accurate heading output even in this harsh environment.
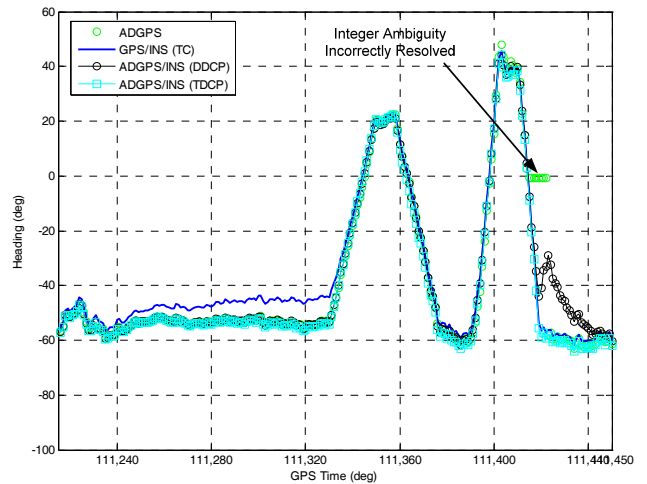

Fig. 16. Heading output during roll motion

4. Concluding Remarks

This paper has proposed an ADGPS/INS integration algorithm using TDCP observables to avoid performance degradation caused by the integer ambiguity error and the cycle slip. A new measurement equation for the Kalman filer has been derived for the TDCP observables. A cycle slip detection algorithm has been also included. Computer simulations have been performed to evaluate performance of the proposed integration algorithm. Simulation results show that the proposed integration algorithm gives a more accurate navigation results even when the ADGPS receiver gives erroneous carrier phase observables due to cycle slip and incorrectly resolved integer ambiguity.

A flight test has been carried out to demonstrate the effectiveness of the proposed algorithm with an automotive grade IMU and multiple antenna GPS receiver. The flight test included roll and pitch maneuverings to evaluate the performance of the proposed algorithm in a high dynamic environment. Outputs of the proposed algorithm were compared with those of a tightly-coupled GPS/INS integration and ADGPS/INS integration with DDCP observables. Flight test results show that the proposed integration algorithm gives better navigation results than other integration algorithms when the ADGPS receiver

provides erroneous attitude outputs. The proposed ADGPS/INS integration system would also be widely used in other applications such as aircraft, military land vehicle, and space vehicle, etc.

References

[1] C. E. Cohen, B. W. Parkinson, "Expanding the Performance Envelope of GPS-based Attitude Determination," *in Proceedings of the ION GPS-91*, pp 1001-1012, Albuquerque, NM, 1991.

[2] C. Park, I. Kim, J. G. Lee., G. I. Jee, "Efficient Ambiguity Resolution with Constraints Equation," *in Proceedings of IEEE PLANS'96*, Atlanta, GO. 1996.

[3] J. Evans, S. Houck, G. McNutt, B. Parkinson, "Integration of a 40 Channel GPS Receiver for Automatic Control Into an Unmanned Airplane," *in Proceedings of the ION GPS-98*, pp 1173-1180, Nashville, TN, 1998.

[4] R. Wolf, G. W. Hein, B. Eissfeller, E. Loehnert, "An Integrated Low Cost GPS/INS Attitude Determination and Position Location System," *in Proceedings of the ION GPS-96*, pp 975-981, Kansas City, MO, 1996.

[5] H. C. Gelderloos, S. I. Sheikh, B. W. Schipper, "GPS Attitude System Integrated with an Inertial System for Space Applications," *in Proceedings of the Digital Avionics Systems Conference, 16th DASC., AIAA/IEEE*, vol 2: 8.1-1-8.1-10, 1997.

[6] D. Gebre-Egziabher, D. R. Hayward, C. D. Powell CD, "A Low-cost GPS/Inertial Attitude Heading Reference System (AHRS) for General Aviation Applications," *in Proceedings of the IEEE PLANS'98*, pp 518-525, 1998.

[7] A. Leick, *GPS Satellite Surveying, 2nd edn.*:John Wiley & Sons, Inc., New York, 1995.

[8] B. Hofmann-Wellenhof, H. Lichtenegger, J. Collins, *Global Positioning System: Theory and Practice, 2nd edn.*: Springer-Verlag, Wien, 1992.

[9] C. Park, *Attitude Determination from GPS Carrier Phase Measurements: Ph.D. Thesis*: Seoul National University, February. 1997.

[10] J. Wendel, O. Meister, R. Monikes, G. F. Trommer, "Time-Differenced Carrier Phase Measurements for Tightly Coupled GPS/INS Integration," *Proceedings of IEEE/ION PLANS 2006*, Apr. 25 - 27, 2006.

[11] B. K. H. Soon, S. Scheding, H.-K. Lee, H.-K. Lee, H Durrant-Whyte, "An approach to aid INS using time-differenced GPS carrier phase (TDCP) measurements," *GPS Solutions*, Vol. 4, No. 4, 2008.

[12] F. V. Graas, S.-W. Lee, "High-accuracy Differential Positioning for Satellite-based Systems without using Code-phase Measurements," *Journal of the Institute of Navigation*, vol. 4, no. 4, pp. 605-618, 1995.

[13] M. Martin-Neira, R. Lucas, M. A. Martinez, "Attitude Determination with GPS: Experimental Results," *IEEE AES Magazine*, pp. 24-29. 1990.

[14] M. Martin-Neira, R. Lucas, "GPS Attitude Determination of Spin Stabilized Satellites," *Proceedings of the Institute of Navigation GPS-92*, Sept. 1992.

[15] I. Nesbo, P. Canter, "GPS Attitude Determination for Navigation," *GPS World*, 1990.

[16] F. V. Grass, M. Brash, "GPS Interferometric Attitude and Heading determination: Initial Flight Test Results," *Navigation: Journal of the ION*, Vol. 38, No. 4, 1992.

[17] J.-C. Juang, G.-S. Huang, "Development of GPS-Based Attitude Determination Algorithms," *IEEE Trans. on AES*. Vol. 33, No. 3, July 1997.

[18] T. S. Bruggemann, *GPS L1 Carrier Phase Navigation Processing: Master Thesis*: Queensland University of Technology, 2005.

[19] S. H. Oh, D.-H. Hwang, S. J. Lee, "An Efficient Integration Scheme for the INS and the Attitude Determination GPS Receiver," *in Proceedings of ION 57th Annual Meeting*, , pp. 334-340, Albuquerque, NM, 2001.

[20] C. Altmayer, "Cycle Slip Detection and Correction by Means of Integrated System," *in Proceedings of the 2000 National Technical Meeting*, pp. 134-144, Anaheim, CA, 2000.

[21] D. Goshen-Meskin, I. Y. Bar-Itzhack, "Unified Approach to Inertial Navigation System Error Modeling," *Journal of Guidance, Control, and Dynamics*, vo1. 15, no. 3, pp. 648-653, 1992.

[22] GPSoft, *Satellite Navigation Toolbox User Guide*: GPSoft LLC., Athens, OH, 1997.

[23] G. Strang, K. Borre, *Linear Algebra, Geodesy, and GPS*: Wellesley-Cambridge Press, Wellesley, MA, 1997.

[24] D Wells, *Guide to GPS Positioning*: Canadian GPS Associates, 1987.

[25] P. S. Maybeck, *Stochastic Models, Estimation and Control*: Academic Press, New York, 1979.

[26] O. L. Colombo, U. V. Bhapkar, A. G. Evans, "Inertial aided Cycle-slip Detection/Correction for Precise, Long-baseline Kinematic GPS," *in Proceedings of the ION GPS-99*, pp. 1915-1922, Nashville, TN, 1992.

Sang Heon Oh is a principal engineer of the Integrated Navigation Division of Hanyang Navicom Co., Ltd., Korea. He received Ph.D. degree from Chungnam National University. His research interests include GPS/INS integration system, Kalman filtering, and military application.

Dong-Hwan Hwang is a professor in the Department of Electronics Engineering, Chungnam National University, Korea. He received his B.S. degree from Seoul National University, Korea in 1985. He received M.S. and Ph.D. degree from Korea Advanced Institute of Science and Technology, Korea in 1987 and 1991, respectively. His research interests include GNSS/INS integrated navigation system design and GNSS applications.

Sang Jeong Lee is a professor in the Department of Electronics Engineering, Chungnam National University, Korea. He received B.S., M.S. and Ph.D. degrees from Seoul National University, Korea in 1979, 1981, and 1987, respectively. His research interests include GNSS receiver design and robust control.
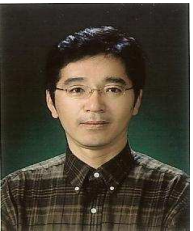
Chansik Park received the B.S., M.S., and Ph.D. degrees in Electrical Engineering from Seoul National University in 1984, 1986, and 1997 respectively. He is currently with the College of Electrical and Computer Engineering, Chungbuk National University, Cheongju, Korea. His research interests include GNSS, SDR, AJ, ITS and WSN